Available online at www.sciencedirect.com
SCIENCE DIRECT®
Planetary and Space Science 53 (2005) 1309–1318
Planetary and Space Science
www.elsevier.com/locate/pss

The advanced Moon micro-imager experiment (AMIE) on SMART-1: Scientific goals and expected results

P. Pinet[a,*], P. Cerroni[b], J.-L. Josset[c], S. Beauvivre[c], S. Chevrel[a], K. Muinonen[d], Y. Langevin[e], M.A. Barucci[f], M.C. De Sanctis[b], Yu. Shkuratov[g], V. Shevchenko[h], P. Plancke[i], B.A. Hofmann[j], M. Josset[k], P. Ehrenfreund[l], Z. Sodnik[m], D. Koschny[m], M. Almeida[m], B. Foing[m]

[a]*UMR 5562 "Dynamique Terrestre et Planétaire", CNRS/Université Paul Sabatier, GRGS (Groupe de Recherche en Géodésie Spatiale), Observatoire Midi-Pyrénées, 14, Avenue Edouard Belin, 31400 Toulouse, France*
[b]*IASF- Area Ricerca Cnr, Via Fosso del Cavaliere, 00133 Roma, Italy*
[c]*Space-X, Centre Space Exploration, Jaquet Droz 1, Neuchâtel, Switzerland*
[d]*Helsinki Observatory, Kopernikuk sentie 1, P.O. Box 14, Finland*
[e]*IAS- Bat. 121, 91405 Orsay, France*
[f]*Observatoire Paris Meudon (OBSPM), Meudon, France*
[g]*Astronomical Institute of Kharkov National University, 35 Sumskaya St, Kharkov 61022, Ukraine*
[h]*Sternberg Astronomical Institute, Moscow 119899, Russia*
[i]*ESA/ESTEC Power and Control Data division, Keplerlaan 1, 2201 Noordwijk, The Netherlands*
[j]*Natural History Museum, Bern, Switzerland*
[k]*Institut de Géologie de l'université de Neuchatel (IGUN), rue Emile Argand 11, Neuchatel, Suisse*
[l]*Leiden Observatory & Austrian Academy of Sciences, P.O. Box 9513, 2300 RA Leiden, The Nederlands*
[m]*ESA Space Science Department (ESA/SSD), Keplerlaan 1, 2201 Noordwijk, The Netherlands*

Received 27 July 2004; received in revised form 14 June 2005; accepted 16 June 2005
Available online 1 September 2005

Abstract

The advanced Moon micro-imager experiment (AMIE) is the imaging system on board ESA mission to the Moon SMART-1; it makes use of a miniaturised detector and micro-processor electronics developed by SPACE X in the frame of the ESA technical programme. The AMIE micro-imager will provide high resolution CCD images of selected lunar areas and it will perform colour imaging through three filters at 750, 915 and 960 nm with a maximum resolution of 46 m/pixel at the perilune of 500 km. Specific scientific objectives will include (1) imaging of high latitude regions in the southern hemisphere, in particular the South Pole Aitken basin (SPA) and the permanently shadowed regions close to the South Pole, (2) determination of the photometric properties of the lunar surface from observations at different phase angles (physical properties of the regolith), (3) multi-band imaging for constraining the chemical and mineral composition of the surface, (4) detection and characterisation of lunar non-mare volcanic units, (5) study of lithological variations from impact craters and implications for crustal heterogeneity. The AMIE micro-imager will also support a Laser-link experiment to Earth, an On Board Autonomous Navigation investigation and a Lunar libration experiment coordinated with radio science measurements.

Keywords: Moon; SMART-1 ESA Mission; Orbital photometry; Spectral imaging

*Corresponding author. Fax: +33 561 33 29 00.
E-mail addresses: patrick.pinet@cnes.fr (P. Pinet), priscio@rm.iasf.cnr.it (P. Cerroni).

0032-0633/$ - see front matter © 2005 Elsevier Ltd. All rights reserved.
doi:10.1016/j.pss.2005.06.003

1. Introduction

Even though the Moon has been extensively studied, there are many domains of lunar science wherein data are still insufficient or interpretations are ambiguous or controversial. In the first period of its life the Moon underwent extensive differentiation processes. The possibility to differentiate a small body like the Moon is strongly related to its formation history. In the process of planetary formation, and for the Moon in particular, the large planetesimals have certainly played a key role (e.g., Safronov, 1969; Pinet, 1985; Tonks and Melosh, 1993); as a striking example, the origin of the Moon has been attributed to a Mars-sized impact on the Earth (e.g., Hartmann and Davis, 1975; Benz et al., 1986; Cameron and Benz, 1991). In the hypothesis of a very hot primordial phase, global melting occurred (magma ocean model), resulting in a complex and heterogeneous crust. Having undergone heavy meteoritic bombardment, these complex crustal rocks occur both as small fragments, eventually re-accreted to form breccias, and as bedrock outcrops as observed by remote sensing (e.g. central peaks of large impact craters, Pieters, 1986, 1993).

The surface of the Moon has been characterised by different episodes of magmatic activity. Early lavas produced by partial melting of the lunar mantle flowed out onto the lunar surface around 4.3–4.0 Ga ago. Most of these ancient deposits (red spot units, pyroclastic deposits and old basaltic deposits) were obliterated by large impacts, buried by basin ejecta or by subsequent mare basalt flooding. Buried mare deposits (cryptomaria) can only be detected by local increases in the iron content of the surface (e.g., Hawke et al., 2003a). The "mare basalts", lying preferentially in the lunar near side, result from lava flows which filled the interior of the large basins from 3.8 to 3.0 Gy ago. Recent studies suggest that volcanic activity continued at a much lower scale in a few areas up to about 1 billion years ago (Hiesinger et al., 2003). Detailed remote sensing investigation of the lunar surface are required for improving our understanding of lunar volcanism (e.g., Chevrel et al., 1999a; Hawke et al., 2003b), setting constraints on the global composition of the Moon and its geological history (Vaniman et al., 1985).

Earth-based and Clementine multi-spectral observations in the UV–VIS–NIR domain, with spatial resolutions in the range of 100 m–1 km have made an important contribution to the spectral characterisation of lunar surface units by providing a first global description of the lateral compositional heterogeneity of the lunar surface and a definition of the main geological units. These observations definitely improved our understanding of the lunar crust structure and nature, and of the emplacement of the maria and cryptomaria. However, these results also suggest that the importance of early lunar volcanism (more than 3.8 Gyr ago), and of impact melting may have been widely underestimated when assessing the evolution and structure of the lunar crust. Optical heterogeneities related to local physical properties of the surface (texture, surface roughness, maturity and cristallinity) at a scale of 100 m or less have not yet been adequately characterised. These goals can be addressed by new generation instruments providing improved spatial resolution and sensitivity.

An opportunity for implementing such investigations has been provided by The "SMART-1" ESA mission to the Moon, which has been successfully launched on September 27th 2003. "SMART" stands for "Small Missions for Advanced Research and Technology", and the main goal of the mission is a validation of Solar Electric propulsion (Racca et al., 2002) which will be implemented in major future missions of ESA such as Bepi Colombo and Solar Orbiter. The science payload also emphasises advances in technology with highly miniaturised experiments. Within a tight mass envelope of 15 kg, this payload will address important issues of lunar science (see, e.g., Foing et al., 2001).

2. The AMIE micro-imager

The advanced Moon micro-imager experiment (AMIE) is the onboard imaging system of the SMART-1 mission. The AMIE micro-imager will acquire broadband images as well as filtered images at three wavelengths (750, 915 and 960 nm). The filters are directly applied onto the CCD, covering an area of 11/16 of the total CCD area, with one 1/16 used by the laser filter at 847 nm, while the remaining 512×512 pixels (i.e., 1/4 of the CCD area) not covered by filters and thus being devoted to broadband imaging (see Fig. 1). It should be noted that while the filters at 750 and 915 nm are two narrow-band filters (respective width of 10 and 30 nm), the filter at 960 nm is a high-pass filter with steep transmission edge, which critically convolves with the negative slope of the CCD spectral response in the longer wavelengths region of the spectrum.

The filter disposition makes it possible to map each region of the sub-spacecraft track at three wavelengths with the two pointing schemes, which will be implemented by SMART-1 (Fig. 1). A more detailed technical description of the AMIE micro-imager and of its subsystems is given in Josset et al. (2003) and Foing et al. (2003). The main characteristics of AMIE are presented in Table 1.

Also, the AMIE capability allows the determination of the photometric properties of the surface. Thus, both geomorphologic studies and geologic interpretation will considerably benefit from the AMIE imaging and multispectral information.

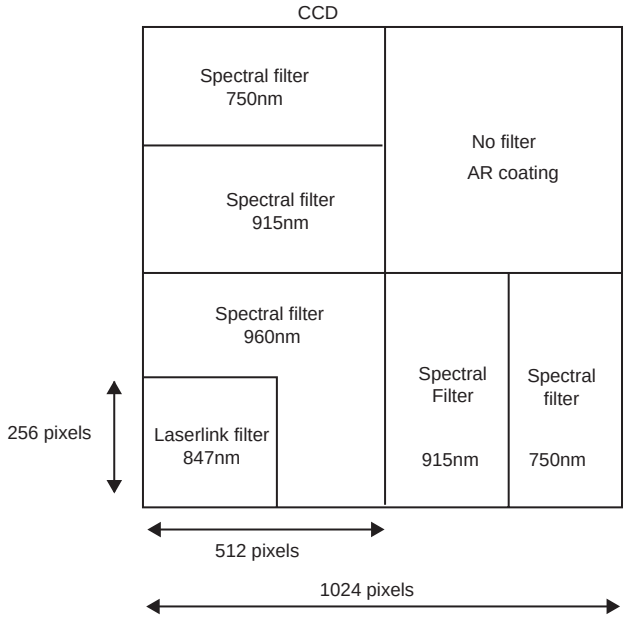

Fig. 1. Layout of the filters on AMIE's CCD.

Table 1
AMIE camera characteristics and performances

Aperture diameter	0.0155 m
Focal length	0.155 m
FOV	$5.3^\circ \times 5.3^\circ$
Detector: CCD (THX7888A)	$14\,\mu m \times 14\,\mu m$
Resolution	0.00576°/pixel; 46 m/pixel at 500 km
Integration time	10 ms–10 s
Dark current	<20 DN/s (6000 e-/s) at 21 °C
Signal-to-noise ratio (SNR)	200–400 (no filter)/80–350 at 915 nm

3. Measurements and expected performances

The spacecraft entered lunar orbit on November 15, 2004. After reaching its final orbit in February 2005 and a commissioning phase until May, 2005, SMART-1 is presently performing an operational phase with science activities in an orbit about 500×3000 km. At a distance of 500 km, the field of view of AMIE ($5.3^\circ \times 5.3^\circ$) corresponds to 46 km on the surface, with a pixel size for the 1024×1024 CCD of 46 m.

The mission plan of SMART-1 is highly complementary to that of Clementine. Indeed, the orbit of Clementine was polar, eccentric, with a pericenter close to the equator. The SMART-1 orbit is also polar and eccentric, but with a pericenter close to the South Pole so that the orbital evolution during the 180 days of nominal mission will provide a good coverage of the $\pm 30^\circ$ southern latitudes. At high-southern latitudes, the AMIE micro-imager will provide a spatial resolution more than 15 times better than Clementine.

When compared to the Clementine UVVIS camera, the AMIE micro-imager has indeed several major advantages: AMIE uses a 1024×1024 pixels CCD, while Clementine was equipped with a 256×256 pixels CCD. Thus, a single AMIE frame acquired from the no-filter area of the CCD (512×512 pixels in size) corresponds, for an equivalent spatial resolution, to 4 Clementine images, giving access to a wider field of view when mapping regional geologic features without the caveats of the mosaicking reduction. It should be noted that even at the lowest altitude of 500 km, the AMIE field of view of 46 km is ideally suited to observe major geologic features. Significant mineralogical diversity can be revealed at the scale of a few tens kilometers (e.g., central peaks of Copernicus).

At the equator, the AMIE resolution will still be close to 150 m per pixel. The resulting images, 150 km × 150 km, will be suitable and very helpful to better understand the photometric characteristics of the lunar surface at different wavelengths. Clementine images are much smaller for this latitude (typically 30 km × 30 km). They were obtained in sequence along a meridian, and consecutive strips (two adjacent orbits) were often obtained under different illumination conditions. The comparison with the AMIE images, obtained with a single exposure, will contribute in the formidable task of patching these small Clementine images into photometrically controlled comprehensive multi-spectral albedo maps of the lunar surface.

In order to obtain multi-colour information, AMIE will image the same geographical area in all three filters, taking advantage of the pushbroom motion of the spacecraft (e.g., Almeida et al., 2002). AMIE, with its multi-band imaging capability, is essential to provide the context for the SIR infrared spectrometer (940–2400 nm; spectral resolution 6 nm; footprint 550 m at 500 km). The correlated interpretation of these two complementary data sets will much enhance the scientific return of each instrument.

Fig. 2 shows as an example the footprint of the AMIE three filters (512×256 pixels each) and non-filter area (512×512 pixels) of the CCD detector for the Reiner Gamma region near the equator (see Fig. 2 for details). Depending on the latitude of the lunar region observed, and therefore the altitude of the spacecraft on its orbit, the swath (full CCD, i.e., 1024×1024 pixels) ranges from 46 km at pericenter (500 km) to 150 km close to the equator, and around 200 km at mid northern latitudes.

It should be also noted that AMIE uses a 10 bits ADC, instead of an 8-bit ADC for Clementine. The large dynamic range of 1023 DN reduces the digital noise. Its main asset is that it eliminates the need for the bewildering number of gain states, acquisition times and offsets used during the Clementine mission, where more than 200 different observation modes had to be implemented, most of which were not calibrated. For

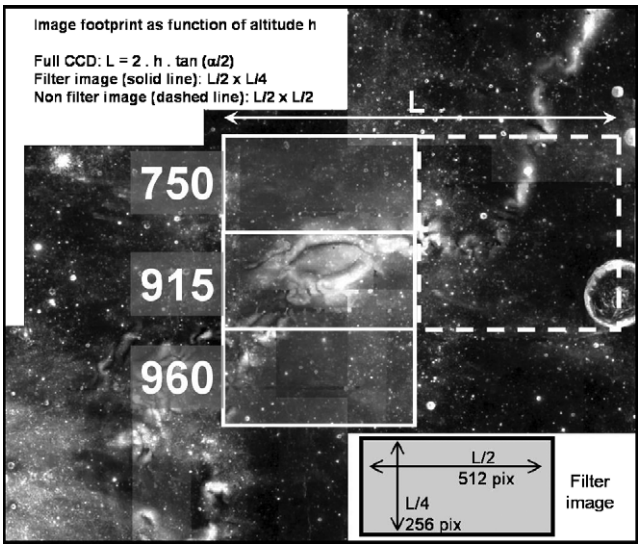

Fig. 2. Example of the footprint of the AMIE three filters (750, 915 and 960 nm; 512×256 pixels each; solid line) and non-filter area (512×512 pixels; dashed line) of the CCD detector (see Fig. 1) superimposed on a Clementine mosaic (not harmonised) of the Reiner Gamma region (about 8°N, 299°E). The swath (L) of the full CCD (1024×1024 pixels) is given by the relation $L = 2.h.\tan(\alpha/2)$ where h is the altitude of the spacecraft (nadir pointing) above the lunar surface and α is the field of view of the AMIE camera. This gives a footprint of $L/2 \times L/4$ (respectively length and height along ground track) for each filter image and $L/2 \times L/2$ for the non-filter image. Assuming an altitude of about 1990 Km at the latitude of Reiner Gamma, one obtains a footprint of 92×92 Km for the non-filter image and 92×46 km for a given filter image.

Fig. 3. Full Moon image produced by AMIE camera during the eclipse of May 4, 2004 from a 100 000 km SMART-1 distance from the Earth.

AMIE, we plan to have far less operative modes, working mainly on the integration time, which has the lowest impact on the photometric response. This will improve the reliability of the data reduction process on the basis of ground calibration.

The acquisition time of AMIE can be adjusted from a few milliseconds to several seconds; this, combined with the large digital dynamics of the instrument and with its intrinsic low noise level (the read noise of the CCD is lower than 100 electrons, hence much less than 1 DN) results in values of the signal-to-noise ratio always sufficiently high to obtain the scientific objectives (Koschny and Almeida , 2003); representative values for the broad band region and for one of the filters with various observation conditions are presented in Table 1.

The high S/N and large dynamic range of AMIE makes it ideally suited for observing permanently shadowed areas and their immediate neighbourhood, and more generally to image regions characterised by very low levels of illumination, with the possibility of imaging the surface of the permanently shadowed areas due to Earth's light: in the most favourable conditions the illumination of these areas from the Earth could reach a value of 5–10 lux.

Fig. 3 shows an image of the Full Moon produced by AMIE micro-imager during the eclipse of May 4, 2004 at a distance of about 100 000 km from the Earth. Fig. 4 shows a first AMIE multi-spectral 960/915 nm ratio image (relative to a highland reference area) of the eastern part of the nearside of the Moon. Images were taken during the first quarter of the Moon on 2004, January, 29, while the spacecraft was still at a distance of about 300 000 km from the Moon. Although these are raw images, the colour ratio shows the presence of a strong mafic absorption for maria, relatively to highlands, consistent with the regional occurrence of iron-rich mare basalts. In particular, the stronger absorption at 960 nm for mare tranquillitatis, relative to other maria (Crisium, Fecunditatis and Nectaris) is consistent with the presence of most iron-rich mare basalts (18–20 wt% FeO) in these regions of the Moon (Lucey et al., 2000).

4. Scientific objectives

The AMIE camera will carry out both scientific and technological objectives; furthermore, it will also be used as a context imager for all other SMART-1 cruise or lunar investigations. The investigation by the AMIE camera will address a number of specific scientific objectives listed below (see also Table 2).

One of the major goals of AMIE will be to acquire high-resolution images of the lunar surface, in total light and for specific spectral bands, under a number of different viewing conditions and geometries.

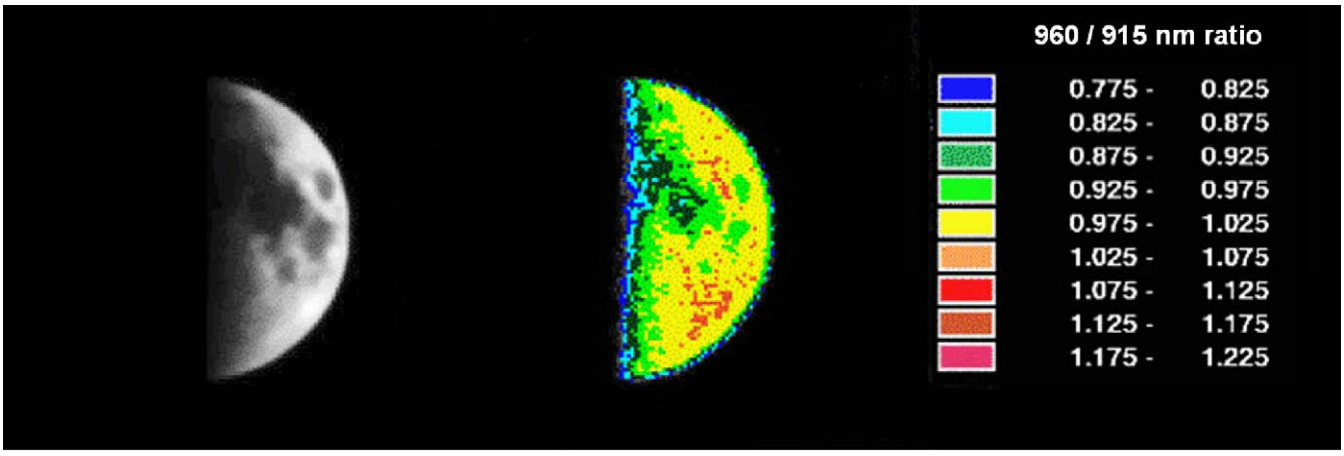

Fig. 4. First AMIE multi-spectral 960/915 nm ratio image of the eastern part of the nearside of the Moon. Colour coding shows variations relative to a highland reference area, with the strongest mafic absorptions reaching 10–15% in mare tranquillitatis, consistent with the regional occurrence of iron-rich mare basalts.

Table 2
Principal types of geological units planned as target for the AMIE camera, and related studies

Type of unit	Example of target	Type of studies
Impact basins		
Floor and rim	South pole-Aitken	Composition and stratigraphy of crustal and basin ejecta materials
Impact craters		
Fresh craters	Copernicus, Tycho	Composition of excavated materials and stratigraphy of the target. Distribution of ejecta materials (rocks versus melts)
Bright rays	Kepler	Composition, surface properties
Floor fractured craters	Gassendi, Taruntius, Petavius	Identification and composition of volcanic deposits in relation with tectonic features
Volcanic units		
Mare basaltic units	young mare deposits in Procellarum	Composition, identification of flow fronts and single flows. Surface properties
Cryptomaria	Schiller-Schickard	Composition and degree of mixing with highlands materials
Pyroclastic deposits (dark mantling deposits)	Aristarchus, Humorum, Orientale, Sinus Medii	Composition, glass content, mode of deposition, identification of source vents, surface physical properties
Non-mare volcanism (domes)	Gruithuisen, Hansteen	Composition, detailed morphology, surface properties
Regolith		
surface properties (photometric studies)	MS2 (Mare Serenitatis standard area), landing sites (Apollo, Luna, Lunakhod), Reiner Gamma and Ingenii swirls	Composition and physical surface properties. Mecanism of regolith evolution (degree of maturity) and modification (lunar swirls)

4.1. Spectral imaging of the lunar regolith

The selected spectral bands allow discrimination between mafic minerals which dominate the mare (revealed by the Fe^{2+} absorption feature at 950 nm) and the feldspar-rich highland materials. The ratio of reflectances 750/950 nm is sensitive to the strength of the 950 nm absorption band and it provides a first-order assessment of relative plagioclase and mafic minerals abundances (e.g., Tompkins and Pieters, 1999). Reliable quantitative methods have been developed for low and medium latitudes by Lucey et al. (1995, 2000); Blewett et al. (1997), and Shkuratov et al. (2003a, b) for separating the effects of soil maturity and iron content on the broad band reflectance properties of the lunar surface. They rely on the relationship between the spectral ratio 950/750 nm and the reflectance at 750 nm. At high latitudes, the local slope is the main controlling parameter of the reflectance, and methods combining visible and near-IR spectral information will be required (Le Mouelic et al., 2002).

There are interesting applications for studying the space weathering of lunar surface material (e.g., Pinet et al., 2000). Lunar surface materials darken, redden and lose spectral contrast with increasing soil maturity, while increasing the mineralogical Fe^{2+} abundance in the

surface material decreases the reflectance of minerals and increases the spectral contrast. Further semi-quantitative ways of discriminating between different mafic-bearing lithologies have been put forward for example by Pieters et al. (2001). The original approach by Tompkins and Pieters (1999) has been extended in this paper and three diagnostic parameters characterising the diagnostic shape of the ferrous band near 1000 nm have been defined. It should be noted that the position of AMIE filters closely mirrors those of the Clementine UVVIS camera, while bringing additional spectral information in the 1000 nm region covered by the Clementine NIR data set; this will allow us to perform similar semi-quantitative mineralogical analysis complementing Clementine UVVIS–NIR results.

For this purpose, a new technique for the determination of lunar surface composition from remote sensing has been recently presented in the context of the SMART-1 mission (Shkuratov et al., 2003a, b). The technique is based on spectral and composition (mineralogy and chemistry) data obtained by the Lunar Soil Characterisation Consortium (Taylor et al., 2000a, b, 2001) for lunar soil samples and the Clementine UVVIS camera data. The distributions of TiO_2, FeO, and pyroxene contents, maturity degree (I_s/FeO), and a characteristic size of particles were mapped. With this technique, one can show the relevance of future AMIE data for quantifying the chemical and mineral composition of the lunar surface (Shkuratov et al., 2003b).

4.2. Detailed high-resolution imaging of the South Pole

The South polar region had been proposed as the focus of European lunar activities by the Lunar Science Advisory Group of ESA on the following grounds: the possibility of ice deposits in the permanently shadowed regions at the South Pole was put forward as a probable explanation for results from the Clementine Bistatic radar experiment (Nozette et al., 1996). Independent results obtained by the Lunar Prospector neutron spectrometer have also identified an excess of hydrogen deposits at the lunar poles (Feldman et al., 1998, 2000), consistent with the presence of possible water ice. The most effective source of the production and accumulation of ice in lunar polar regions is likely to be comets (Shevchenko, 1999). It has been proposed that ice deposits could only survive in "double shadow" regions, i.e. small craters located in permanently shadowed areas, which protect the deposit from sunlight diffused by the rims. The shaded zone near the South Pole is located below the absolute datum level, the height of the closest rim being about 3 km. Thus, in this region, the "solar horizon" is always 1–2° below the topographic horizon (Chikmachev and Shevchenko, 1999). Estimates of extent of "double shadow" areas show that they could represent up to 10^4 km^2 (Petrov et al., 2003). During its mission lifetime around the Moon, the AMIE camera will produce repeated high-resolution coverage of the polar regions under different geometrical conditions ("Sun–lunar area–spacecraft") and it will thus provide us with a precise assessment of the characteristics of permanently shadowed areas.

The South Pole is on the rim of a major geological feature discovered by Clementine, the South Pole Aitken basin (SPA), the largest impact basin on the Moon with a diameter of 2500 km, and a depth of 12 km (e.g., Zuber et al., 1994). From the Galileo and the Clementine spectral data, it has been shown that the basin floor, which is mostly composed of basin ejecta deposits and small deposits of mare basalts, exhibits a lower albedo and higher mafic mineral abundances than the surrounding highlands (Petro and Pieters, 2004). Because of its size, and of this mafic anomaly, it has been suggested that deep crustal and mantle materials have been excavated and deposited during the impact event that formed the Aitken basin (e.g., Head et al., 1993; Spudis et al., 1994; Pieters et al., 1997; Lucey et al., 1998; Pieters et al., 2001). However, the composition of the materials forming the SPA basin floor, inferred from both the spectral Clementine data and the geochemical Lunar Prospector data, is still a matter of debate (e.g., Pieters et al., 1997, 2000; Lucey et al., 1998; Blewett et al., 2000; Chevrel et al., 1999b, 2000, 2002; Lawrence et al., 1999).

The determination of the composition of the materials found in the SPA basin is important because it will give important constraints to the processes of formation of the large basins on the Moon and the evolution of the crust. There is a strong interest in investigating at close range the mineral composition of ejecta which provide a vertical sounding of the farside crust down to several tens of km. AMIE will directly contribute to the characterisation of surface mineralogy and geology in the SPA region, in combination with other elements of the payload (SIR spectrometer, D-CIXS X-ray spectrometer); this represents an important task in preparation to a planned sample return mission in SPA. As an example, the AMIE multi-spectral capability could be used to search for cryptomaria around dark halo craters in the SPA region (see, e.g., Blewett et al., 1999). These observations would take advantage of the rather high resolution at the southern latitudes, and would be complemented by the full NIR spectra provided by SIR (Basilevsky et al., 2004) and by elemental abundance analysis by D-CIXS.

4.3. Study of lithological compositional diversity from impact craters

Compositional heterogeneities have been observed in morphological structures (central peaks, floor, walls, rims) of impact craters. For instance, Tompkins and

Pieters (1999) discuss the presence of high-Ca pyroxene-bearing rocks on the walls of Tycho crater, indicating that gabbroic plutons in the crust might have been exposed as a result of the impact process. Given the AMIE camera capabilities, it would be important to improve, at a spatial resolution of 50 m/pixel, the characterisation of structural lithological variations revealed earlier at the sub-kilometer scale by telescopic and Clementine images on the walls of large impact craters, such as Copernicus (Pinet et al., 1993; Pieters et al., 1994; Le Mouelic and Langevin, 2001). Complex lithological variations have also been found in craters such as Aristarchus (e.g., Pinet et al., 1999; Le Mouélic et al., 2000; Chevrel et al., 2004). Indeed, a global survey of central peaks of 109 craters in the diameter range from 40 to 180 km (Tompkins and Pieters, 1999) has shown that 40% of them exhibit multiple lithology, considered to be associated with vertical and lateral differences in composition of the lunar crust. In general, craters found within impact basins are more heterogeneous than highland craters, with the notable exception of Tycho, which exhibits the most mafic central peak. Three distinct, relatively mafic units are visible at Stevinus with sharp contacts showing variations in albedo and colour. At Theophilus, the central peaks display both anorthositic and troctolitic composition.

Higher resolution data from AMIE, combined with SIR, could identify combination of smaller, lithologically distinct units within their central peaks and walls. Classification of mapped lithological units ranging from pure feldspathic to feldspathic and/or mafic materials could be done on the basis of the reflectance ratio 750/1000 nm, while for more detailed compositional studies the AMIE camera should provide the imaging support for detailed spectral analysis by SIR (Basilevsky et al., 2004) and elemental analysis by D-CIXS. The characterisation and the distribution of fresh crater materials (including the ejecta blanket), respectively at high spatial and spectral resolution by AMIE and SIR, will also contribute to better document the processes of excavation and production of impact materials (e.g., abundance of rocks versus melt products).

4.4. Detection and characterisation of the ancient lunar non-mare volcanism

While lunar mare volcanism appears both widespread and well documented, little is known about the emplacement of lunar non-mare volcanic units before and during the period of mare basaltic volcanism. As with mare volcanism, the existence of non-mare volcanism has equally major implications for the thermal history and crustal evolution of the Moon, in relation with the role played by the volatile elements. The best candidates today for non-mare volcanic deposits are a number of small lunar areas called red spots. These are anomalous areas primarily characterised by a relatively high albedo and a strong absorption in the UV relative to the visible (Malin, 1974; Wood and Head, 1975; Chevrel et al., 1999a; Hawke et al., 2003a, b).

The AMIE camera will provide high-spatial resolution imaging associated with different geometry conditions of observation and combined with multi-spectral mapping. These data will document the mineralogy, morphology and surface physical characteristics, while more detailed compositional analysis from spectrophotometric properties could rely on data from SIR (Basilevsky et al., 2004). For example, it is expected to detect compositional variations within the volcanic domes in relation with surface structures (lava flows and/or landslides) and textures, and thus to document the style of volcanism and the nature of materials emplaced.

4.5. Physical properties of regolith

The lunar regolith is a complex end-product of the bombardment history of the Moon. Its constituents have been fractured, melted, welded (forming complex breccias), displaced during the major cratering events and reworked by smaller impacts. The study of the depth distribution and physical properties of the regolith requires high-resolution imaging. Observations planned at different phase angles during the SMART-1 mission will allow us to study the photometric properties of the regolith, from which physical properties of the surface can be inferred (see, e.g., Pinet et al., 1998; Shkuratov et al., 1999, 2002, 2003c; Muinonen et al., 2002; Cord et al., 2002, 2003a, b; Shevchenko et al., 2003; Pugacheva and Shevchenko, 2003; Kreslavsky and Shkuratov, 2003).

Three different kind of photometric studies with the AMIE camera of SMART-1 mission will be possible: (1) determination of the phase function and search for photometric anomalies; (2) characterisation of the opposition spike; (3) detailed study of photometric function in the spot pointing mode of SMART-1. The first type of investigation will be particularly interesting close to fresh impact craters, where photometric anomalies have implications on the regolith gardening rate and the recent projectile flux; It will also be possible to investigate regolith anomalies associated with swirls, ejecta fields and deposits, and possible evidence for recent seismic events. The second type of investigation makes it possible to study regional variations of the characteristic soil particle size and particle aggregate structure. The third type of investigation (tracking mode or spot pointing) will provide a detailed understanding of the photometric function with implications on the meso-scale structure of the lunar surface. The specific requirements of photometric studies are the following:

- At least two images of the same scene are needed for characterising the phase function. As the phase angle

difference should be comprised between 15° and 30°, the best choice of the phase angles is 10–20° for the first image and 30–50° for the second image; pairs of AMIE images are clearly preferred, but one could also use images from the Clementine data set.

- Two images of the same scene are needed as well to study the opposition spike, one of which should contain the zero phase angle point, while the other should be taken at a phase angle of 10–40°; also, in this case, one of the two images could be taken from the Clementine data set if cross-correlation problems can be solved satisfactorily.
- The spot pointing mode requires taking a set of AMIE images of the same scene while the spacecraft is moving along its orbit with motion compensation; including the zero phase angle point into the imaging sequence would increase the scientific output of this mode. A flat surface is necessary for photometric mapping with the AMIE camera. Regions for mapping with the highest priority are the Apollo-11, -12, -14, and -16 landing sites. Other prospective regions are also: Surveyor 1, 3, 5, 6, and 7, Luna 16, 17 (Lunokhod 1), 20, 21 (Lunokhod 2), and 24 landing sites, swirls, selected typical mare areas, and areas that have been imaged with Clementine at the opposition.

At the local scale, the photometric properties of the lunar regolith are still poorly known (Helfenstein and Shepard, 1999). Their detailed study is a key for understanding the soil maturation process occurring in the regolith, which result from impact communition, the accumulation of agglutinates, and the production of reduced iron from vacuum reduction of Fe^{2+} in minerals and glasses. As an example, the puzzling case of the Reiner Gamma formation suggests that areas may exist on the Moon where the regolith could present locally unusual optical, mechanical, and magnetic properties (Pinet et al., 2000; Pinet et al., 2004). High-resolution orbital surveys will improve our understanding of the stratigraphy and evolution of the regolith.

5. Conclusion

The AMIE experiment onboard the SMART-1 mission is a new generation of advanced imaging system, combining a miniaturised detector with micro-processor electronics which result in low mass and power requirements. Important scientific objectives will be addressed, which include: (i) the detailed imaging of high latitude areas in the southern hemisphere (South Pole—Aitken basin and permanently shadowed regions close to the pole), (ii) the study of photometric properties of the lunar surface from observations at different phase angles for the determination of the characteristics of the regolith, (iii) the determination of new constraints on the chemical and mineral composition of the regolith upper layer, (iv) the detection and characterisation of lunar non-mare volcanic units, (v) the study of the local lithological variations from impact craters and implications for crustal heterogeneity.

AMIE will provide the context support for experiments dedicated to compositional studies, i.e. the detailed spectroscopic survey performed by SIR and the geochemical elemental analysis carried out by D-CIXS. This will require a coordinated observation strategy so as to obtain a comprehensive coverage of targets of interest. With its complementary set of instruments, SMART-1 will provide an interesting testbed of data analysis strategies for the more ambitious and systematic survey which will be provided by the LSPIM package (high-resolution spectrometer embedded in the field of view of a multi-spectral camera) on the japanese SELENE mission, to be launched in 2007.

The AMIE micro-imager will also support a Laser-link experiment to Earth at 0.83 μm, an On Board Autonomous Navigation investigation and a Lunar libration experiment coordinated with radio science measurements.

Acknowledgments

P. Pinet, S. Chevrel and Y. Langevin acknowledge the support of the French Space Agency (CNES). P. Cerroni and M. C. De Sanctis acknowledge the contribution by the Italian Space Agency (ASI). This work has also been partially supported by INTAS Grant # 2000-0792 (Y. Shkuratov, V. Shevchenko, K. Muinonen, P. Pinet). We thank Y.Daydou and N. Guyennon for their technical assistance. We are grateful to Dr. A. Basilevsky and another anonymous reviewer for their useful comments of the manuscript.

References

Almeida, M., Foing,B., Vilar, E., Heather, D., Koschny, D., Marini, A., 2002. Smart-1 Science Experiments Co-ordination, ESA internal report, 6pp.

Basilevsky A. T., Keller, H. U., Nathues, A., Mall, U., Hiesinger, H., Rosiek, M., 2004. Scientific objectives and selection of targets for the SMART-1 mission Infrared Spectrometer (SIR), Planet. Space Sci., submitted for publication.

Benz, W., Slattery, W.L., Cameron, A.G.W., 1986. The origin of the Moon and the single impact hypothesis I. Icarus 66, 515–535.

Blewett, D.T., Lucey, P.G., Hawke, B.R., Jolliff, B.L., 1997. Clementine images of the lunar sample-return stations: refinement of FeO and TiO_2 mapping techniques. J. Geophys. Res. 102 (E7), 16319–16325.

Blewett, D.T., Taylor, G. J., Lucey, P.G., Hawke, B.R., Gillis, J.J., 1999. High-resolution quantitative remote sensing of South-Pole Aitken basin. LPSC XXX, Abstract n. 1438.

Blewett, D.T., Lucey, P.G., Hawke, B.R., Holtzmann, J., Taylor, G.J., Lawrence, D.J., 2000. Compositional studies of the South Pole-Aitken basin. LPSC XXXI Abstract #1501.

Cameron, A.G.W., Benz, W., 1991. The origin of the Moon and the single impact hypothesis IV. Icarus 92, 204–216.

Chevrel, S.D., Pinet, P.C., Head, J.W., 1999a. Gruithuisen domes region: a candidate for an extended nonmare volcanism unit on the Moon. J. Geophys. Res. 104, 16515–16529.

Chevrel, S.D., Pinet, P.C., Barreau, G., Daydou, Y., Richard, G., Maurice, S., Feldman, W.C., 1999b. Integration of the UV–VIS spectral Clementine data and the gamma-ray Lunar Prospector data: preliminary results concerning FeO, TiO2 and Th abundances of the lunar surface at global scale. Workshop on: The New Views of the Moon II: Understanding the Moon through the integration of diverse datasets. LPI Contribution No. 980, Lunar and Planetary Institute, Houston, TX.

Chevrel, S.D., Pinet, P.C., Barreau, G., Daydou, Y., Maurice, S., Feldman, W.C., Lawrence, D.J., Lucey, P.G., 2000. Fe, Ti and Th abundances of the lunar surface at global scale from UV-VIS spectral Clementine and the gamma-ray Lunar Prospector data. LPSC XXXI Abstract #1629.

Chevrel, S.D., Pinet, P.C., Daydou, Y., Maurice, S., Lawrence, D.J., Feldman, W.C., Lucey, P.G., 2002. Integration of the Clementine UV–VIS spectral reflectance data and the Lunar Prospector gamma-ray spectrometer data: a global-scale multielement analysis of the lunar surface using iron, titanium, and thorium abundances. J. Geophys. Res. 107, E12.

Chevrel, S.D., Pinet, P.C., Daydou, Y., Baratoux, D., Costard, F., Le Mouélic, S., Langevin, Y., Erard, S., 2004. Compositional and structural study of the aristarchus plateau from integrated Uv–Vis–NIR spectral data. In: Proceedings of 35th LPSC.

Chikmachev, V.I., Shevchenko, V.V., 1999. A macromodel of the lunar South-pole-region relief. Sol. System Res. 33, 18–28.

Cord, A.M., Pinet, P.C., Daydou, Y., Stankevich, D., Shkuratov, Yu., 2002. Planetary regolith surface analogs and mesoscale topography: optimized determination of Hapke parameters using multi-angular spectro-imaging laboratory data. In: Proceedings of Solar System Remote Sensing Conference, LPI contribution No 1129, Pittsburgh, september 2002, pp. 17–18.

Cord, A.M., Pinet, P.C., Daydou, Y., Chevrel, S., 2003a. Experimental determination of the Hapke shadowing function parameter for planetary regolith surface analogs. Lunar Planet. Sci. 34th. #1349, Houston, 2003a.

Cord, A.M., Pinet, P.C., Daydou, Y., Chevrel, S., 2003b. Planetary regolith surface analogs: optimized determination of Hapke parameters using multi-angular spectro-imaging laboratory data. Icarus 165, 414–427.

Feldman, W.C., Maurice, S., Binder, A.B., Barraclough, B.L., Elphie, R.C., Lawrence, D.J., 1998. Fluxes of fast and epithermal neutron from Lunar prospector: evidence for water ice at the lunar poles. Science, 1496–1500.

Feldman, W.C., Lawrence, D.J., Elphie, R.C., Barraclough, B.L., Maurice, S., Genetay, I., Binder, A.B., 2000. Polar hydrogen deposits on the Moon. J. Geophys. Res. 105, 4175.

Foing, B.H., Heather, D.J., Almeida, M., the SMART-1 Science and Technology working Team, 2001. The science goals of ESA's SMART-1 mission to the Moon. Earth, Moon Planets 85–86, 523–531.

Foing, B.H., Raca, G.D., Marini, A., Heather, D.J., Koschny, D., Grande, M., Huovelin, J., Keller, H.U., Nathues, A., Josset, J.L., Malkii, A., Schmidt, W., Noci, G., Birkl, R., Iess, L., Sodnik, Z., McManamon, P., the SMART-1 STWT, 2003. SMART-1 mission to the Moon: technology and science goals. Adv. Space Res. 31 (11), 2323–2333.

Hartmann, W.K., Davis, D.R., 1975. Satellite-sized planetesimals and lunar origin. Icarus 24 (4), 504–515.

Hawke, B.R., Blewett, D.T., Bussey, D.B.J., Giguere, T.A., Lawrence, D.J., Lucey, P.G., Smith, G.A., Spudis, P.D., Taylor, G.J., 2003a. Geochemical anomalies in the lunar highlands. Lunar Planet. Sci. Conf. XXXIV, 1198.

Hawke, B.R., Lawrence, D.J., Blewett, D.T., Lucey, P.G., Smith, G.A., Spudis, P.D., Taylor, G.J., 2003b. Hansteen Alpha: a volcanic construct in the lunar highlands. J. Geophys. Res. 108 (E7), 5069.

Head, J.W., Murchie, S., Mustard, J.F., Pieters, C.M., Neukum, G., McEwen, A., Greeley, R., Nagel, E., Belton, M.J.S., 1993. Lunar impact basins: new data for the wetern and farside (Orientale and South Pole Aitken basins) from the first Galileo Flyby. GJ. Geophys. Res. 98 (E9), 17,149–17,181.

Hiesinger, H., Head, J.W., Wolf, U., Jaumann, R., Neukum, G., 2003. Ages and stratigraphy of mare basalts in Oceanus Procellarum, Mare Nubium, Mare Cognitum and Mare Insularum. J. Geophys. Res. 108 (E7), 5065.

Helfenstein, P., Shepard, M., 1999. Submillimeter-scale topography of the lunar regolith. Icarus 141, 107–131.

Josset, J.-L., Beauvivre, S. 2003. AMIE Team, Science Goals and Expected Results from the SMART-1 AMIE Multi-Coulour Micro-Camera, EGS Nice.

Koschny, D., Almeida, M., 2003. Advanced moon Imaging Experiment: Signal to Noise Ratio calculations from ground-based observations, Esa internal document S1-AMIE-RSSD-TN-002, 13pp.

Kreslavsky, M., Shkuratov, Yu., 2003. Photometric anomalies of the lunar surface: results from Clementine data. J. Geophys. Res. 108 (E3) 1-1–1-13.

Lawrence, D.J., Feldman, W.C., Barraclough, B.L., Maurice, S., Binder, A.B., Lucey, P.G., 1999. Iron abundances on the Moon as seen by the Lunar Prospector gamma-ray spectrometer. Workshop on:The New Views of the Moon II: Understanding the Moon through the integration of diverse datasets, LPI Contribution No. 980, Lunar and Planetary Institute, Houston, TX.

Le Mouelic, S., Langevin, Y., 2001. The olivine at the lunar crater Copernicus, as seen by Clementine NIR data. Planet. Space Sci. 49, 65–70.

Le Mouelic, S., Langevin, Y., Erard, S., Pinet, P.C., Daydou, Y., Chevrel, S., 2000. Discrimination between maturity and composition of lunar soils from integrated Clementine UVVis-NIR data. Application to Aristarchus Plateau. J. Geophys. Res. 105 (E4), 9445–9455.

LeMouélic, S., Lucey, P.G., Langevin, Y., Hawke, B.R., 2002. Calculating iron contents of lunar highland materials surrounding Tycho crater from integrated Clementine UV–visible and near-infrared data. J. Geophys. Res. 107, 4–10.

Lucey, P.G., Taylor, G.J., Malaret, E., 1995. Abundance and distribution of iron on the Moon. Science 268, 1150–1153.

Lucey, P.G., Taylor, G.J., Hawke, B.R., 1998. FeO and TiO_2 concentrations in the South of Pole-Aitken basin: Implications for mantle composition and basin formation. J. Geophys. Res. 103 (E2), 3701–3708.

Lucey, P.G., Blewett, D.T., Jolliff, B.L., 2000. Lunar iron and titanium abundance based on final processing of Clementine ultraviolet–visible images. J. Geophys. Res. 105 (E8), 20,297–20,305 20,3701–20,3708.

Malin, M.C., 1974. Lunar red spots: Possible pre-mare materials. Earth Planet. Sci. Lett. 21, 331–341.

Muinonen, K., Shkuratov, Yu., Ovcharenko, A., Piironen, J., Stankevich, D., Miloslavskaya, O., Keraenen, S., Josset, J.-L., 2002. The SMART-1 AMIE experiment: implication to the lunar opposition effect. Planet. Space Sci., 1339–1344.

Nozette, S., Lichtenberg, C.L., Spudis, P., Bonner, R., Ort, W., Malaret, E., Robinson, M., Shoemaker, E.M., 1996. The Clementine Bistatic Radar experiment. Science 274 (5292), 1495–1498.

Petro, N., Pieters, C.M., 2004. Surviving the heavy bombardment: ancient material at the surface of South Pole-Aitken. J. Geophys. Res. 109, E06004.

Petrov, D., Shkuratov, Yu., Stankevich, D., Shevchenko, V., Kozlova, E., 2003. Area of cold traps on the lunar surface. Sol. System Res. 37, 260–265.

Pieters, C.M., 1986. Composition of the lunar highland crust from near-infrared spectroscopy. Rev. Geophys. 24, 557–578.

Pieters, C.M., 1993. Compositional diversity and stratigraphy of the lunar crust derived from reflectance spectroscopy. In: Pieters, C.M., Englert, P.A.J. (Eds.), Remote Geochemical Analysis: Elemental and Mineralogical Composition. Cambridge University Press, New York, pp. 309–339.

Pieters, C.M., Staid, M.I., Fisher, E.M., Tompkins, S., He, G., 1994. A sharper view of impact craters from Clementine data. Science 266, 1844–1848.

Pieters, C.M., Tompkins, S., He, G., Head, J.W., Hess, P.C., 1997. Mineralogy of the mafic anomaly in the South Pole-Aitken basin (SPA); Implications for the excavation of the lunar mantle. Geophys. Res. Lett. 24, 1903–1906.

Pieters C.M., Head, J.W., Tompkins, S., 2000. Rock types of South Pole-Aitken: implications for basin evolution. LPSC XXXI, Abstract #1438.

Pieters, C.M., Head, J.W., Gaddis, L., Jolliff, B., Duke, M., 2001. Rock types of South Pole—Aitken basin and extent of basaltic volcanism. J. Geophys. Res. 106, 28001–28022.

Pinet, P.C., 1985. Lunar impact flux distribution and global asymmetry revisited. Astron. Astrophys. 151, 222–234.

Pinet, P.C., Chevrel, S., Martin, P., 1993. Copernicus—a regional probe of the lunar interior. Science 260, 797–801.

Pinet, P.C., Chevrel, S.D., Martin, P.D., Daydou, Y.H., 1998. Interest of high resolution morphology imaging by Lunar-A (LIC camera): examples of the Aristarchus Plateau and Mare Humorum regions. Third International Conference of the Exploration and Utilization of the Moon, (Invited paper), Moscow.

Pinet, P.C., Chevrel, S.C., Daydou, Y.H., Lemouelic, S., Langevin, Y., Erard, S., 1999. Aristarchus crater spectroscopic heterogeneity from Clementine UV-VIS-NIR data. In: Lunar and Planetary Science Conference, 30th, Houston, Texas, Contribution 1555, 2pp.

Pinet, P.C., Shevchenko, V.V., Chevrel, S.D., Daydou, Y., Rosemberg, C., 2000. Local and regional lunar regolith characteristics at Reiner Gamma Formation: optical and spectroscopic properties from Clementine and Earth-based data. J. Geophys. Res. 105, 9457–9475.

Pinet, P.C., Cord, A.M., Chevrel, S., Daydou, Y., 2004. Optical response and surface physical properties of the lunar regolith at Reiner Gamma formation from Clementine orbital photometry: derivation of the Hapke parameters at local scale. Lunar Planet. Sci. 35th. Abstract # 1660 Houston.

Pugacheva, S.G., Shevchenko, V.V., 2003. Photometry of the Moon with AMIE/SMART-1: photometric parameter as roughness index. LPSC XXXIV, 1112–1113.

Racca, G., Marini, A., Stagnaro, L., Van Dooren, J., di Napoli, L., Foing, B.H., and the SMART-1 Team, 2002. SMART-1 mission description and development status. Planet. Space Sci. 50, 1323–1337.

Safronov, V.S., 1969. Evolution of protoplanetary cloud and formation of the Earth and Planets, Nauka Moskow, (Translation, NASA TT F-67, 206, 1972).

Shevchenko, V.V., 1999. On the cometary origin of the lunar ice. Sol. System Res. 33, 400–408.

Shevchenko, V.V., Pinet, P., Chevrel, S., Daydou, Y., 2003. Lunar photometry and composition of ejecta terrains with AMIE/SMART-1. LPSC XXXIV, 1113–1114.

Shkuratov, Yu., Kreslavsky, M., Ovcharenko, A., Stankevich, D., Zubko, E., Pieters, C., Arnold, G., 1999. Opposition effect from Clementine data and mechanisms of backscatter. Icarus 141, 132–155.

Shkuratov, Yu.G., Kreslavsky, M.A., Foing, B.H., 2002. Photometric studies of the Moon with AMIE/SMART-1. 34th COSPAR Scientific assembly. The second World Space Congress. Houston TX USA 10-19 October 2002. Abstract # COSPAR02-A-01510.

Shkuratov, Yu., Pieters, C., Omelchenko, V., Stankevich, D., Kaydash, V., Taylor, L., 2003a. Estimates of the lunar surface composition with Clementine images and LSCC data. 34th Lunar Planetary Science Conference. Abstract # 1258. LPI Houston.

Shkuratov, Yu., Stankevich, D., Kaydash, V., Omelchenko, V., Pieters, C., Pinet, P., Chevrel, S., Daydou, Y., Foing, B., Sodnik, Z., Josset, J.-L., Taylor, L., Shevchenko, V., 2003b. Composition the lunar surface as will be seen from SMART-1: simulation using Clementine data. J. Geophys. Res. Planet 108 (E4) 1-1–1-12.

Shkuratov, Yu.G., Kreslavsky, M.A., Stankevich, D.G., Kaydash, V.G., Pinet, P., Shevchenko, V.V., Foing, B.H., Josset, J.-L., 2003c. The SMART-1 mission: photometric studies of the Moon with the AMIE camera. Sol. System Res. 37, 251–259.

Spudis, P.D., Reisse, R.A., Gillis, J.J., 1994. Ancient multiring basins and the Moon revealed by Clementine laser altimetry. Science 266, 1848–1851.

Taylor, L.A., Morris, R.V., Pieters, C., Patchen, A., Taylor, D.H., Keller, L.P., Wentworth, S., McKay, D.S., 2000a. Chemical Characterization of Lunar Mare Soils. Lunar Planet. Sci. XXXI [CD-Rom] abstract 1697.

Taylor, L.A., Patchen, A., Taylor, T.D.H., Morris, R.V., Pieters, C., Keller, L.P., Wentworth, S., McKay, D.S., 2000b. Mineralogical Characterization of Lunar Mare Soils. Lunar Planet. Sci. XXXI [CD-Rom], abstract 1706.

Taylor, L.A., Pieters, C.M., Morris, R.V., Keller, L.P., McKay, D.S., 2001. Lunar mare soils: space weathering and the major effects of surface-correlated nanophase Fe. J. Geophys. Res. 106 (E11), 27,985–28,000.

Tompkins, S., Pieters, C., 1999. Mineralogy of the lunar crust: results from Clementine. Meteorit. Planet. Sci. 34, 25–41.

Tonks, W.B., Melosh, H.J., 1993. Magma Ocean formation due to giant impacts. J. Geophys. Res. 98, 5319–5333.

Vaniman, D.T., Heiken, G., Taylor, G.J., 1985. A closer look at lunar volcanism from a base on the Moon. In: Mendell, W.W. (Ed.), Lunar bases and space activities of the 21th century. Lunar and Planetary Inst., Houston, USA, pp. 211–222.

Wood, C.A., Head, J.W., 1975. Geologic setting and provenance of spectrally distinct pre-mare material of possible volcanic origin. Conference on Origin of Mare basalts. Lunar Science Institute.

Zuber, M.T., Smith, D.E., Lemoine, F.G., Neumann, G.A., 1994. The shape and internal structure of the Moon from the Clementine mission. Science 266, 1839–1843.